2016

Sulcal and gyral distribution of cortical white matter neurons in macaque monkey

BOSTON UNIVERSITY

SCHOOL OF MEDICINE

Thesis

SULCAL AND GYRAL DISTRIBUTION OF CORTICAL WHITE MATTER NEURONS IN MACAQUE MONKEY

by

DANIEL LEE

B.S., New York University, 2009

Submitted in partial fulfillment of the

requirements for the degree of

Master of Science

2016

Approved by

First Reader _____

Kathleen Rockland, Ph.D.
Research Professor of Anatomy and Neurobiology

Second Reader _____

Maryann MacNeil, M.A.
Instructor of Anatomy and Neurobiology

SULCAL AND GYRAL DISTRIBUTION OF WHITE MATTER NEURONS IN MACAQUE MONKEY

DANIEL LEE

ABSTRACT

Purpose: To compare white matter neuron density across 3 regions, prefrontal, temporal, and posterior parietal (PFC, TE, PP) in macaque monkey, with further analysis of subdivisions within the gyral white matter.

Methods: Histological tissue from three adult macaque monkeys, previously prepared with the neuron-specific pan-neuronal marker Neuronal-N, was used for analysis. Tissue was digitized and processed electronically to investigate cross- and intra-regional differences in the distribution of white matter neurons.

Results: Statistical analysis showed significant differences across all regions sampled and across most intra-regional subdivisions, although the more conservative post-hoc tests failed to find significant differences between specific regions.

Conclusions: The results of the current study support regional differences. Further studies using a larger sample size may help elucidate the relatively unknown properties of white matter neurons.

TABLE OF CONTENTS

LIST OF TABLES

LIST OF FIGURES

LIST OF ABBREVIATIONS

ANOVA ..... Analysis of variance

DAB ..... 3-3'-diaminobenzidine

dMRI ..... Diffusion magnetic resonance imaging

GABA ..... Gamma-aminobutyric acid

IgG ..... Immunoglobulin G

mm ..... Millimeter

NADPH ..... Nicotinamide adenine dinucleotide phosphate

Neu-N ..... Neuronal N

NGS ..... Normal goat serum

NHP ..... Nonhuman primate

NOS ..... Nitric oxide synthase

PFC ..... Prefrontal cortex

PP ..... Posterior parietal lobe

ROI ..... Region of interest

SEM ..... Standard error of the mean

STS ..... Superior temporal sulcus

sWM ..... Superficial white matter

TBS ..... Tris buffered saline

TE ..... Temporal lobe

TEU ..... Temporal lobe above superior temporal sulcus

TEL ..... Temporal lobe below superior temporal sulcus

Tris ..... Tris(hydroxymethyl)aminomethane

WMN ..... White matter neurons

INTRODUCTION

Early History

Neurons in the white matter were first described by the German-Austrian neuropathologist Theodor Meynert in 1867, who wrote on the "solitary neurons" he had discovered in the subcortical white matter of the adult brain (Figure 1. Judaš, 2010; Meynert, 1867). Meynert believed his discovery to be a normal finding, and inferred that these neurons participated in corticocortical circuits (Judaš, 2010; Meynert, 1867). White matter neurons were further described by the Spanish neuroscientist Ramón y Cajal, who is credited with coining the alternative term for white matter neurons (WMNs), interstitial neurons (Judaš, 2010). As Judaš writes, the term interstitial, itself, was widely used in the 19th century to refer to cells in any "between-space" and Cajal was probably just the first to apply it to neurobiology. It is of note, however, that Cajal initially did not ascribe this term to the cells in the subcortical white matter but rather to all kinds of non-cortical neurons such as those found in the gut and pancreas (Judaš, 2010). Cajal discovered that these subcortical neurons had ascending axons that projected to the grey matter and believed the cells to simply be cortical neurons that had been displaced into the immediately adjacent white matter (Cajal, 1899-1904). In fact, it was only in an update in a translation of his 1895 work on the cerebellum that Cajal first used the term "interstitial cells" to differentiate between large stellate cells found in cerebellar white matter and marginal cells found at the cortico-white matter border (Cajal, 1895, 1896; Judaš, 2010).

Figure 1. (a) Coronal section (from posterior parietal region) after immunohistochemistry and digitalization. Arrow shows the approximate border between cortical Layer VI and superficial white matter as marked by substantial decrease in cell density. (b) Higher magnification image of neurons as these appear when stained with Neu-N. The black line represents the approximate border of white matter and grey matter.

Functions

It wasn't until almost a century later in 1980 that Kostovic and Rakic suggested that the term "interstitial cells" could also be applied to similar cells in regions other than the white matter of the cerebellum (Kostovic & Rakic, 1980). Kostovic and Rakic also suggested that these interstitial neurons were the surviving "remnant" of fetal subplate neurons, known to decrease in density as the brain matures (Kostovic & Rakic, 1990). This subplate refers to the transient layer found subjacent to the developing cortex, which

plays a key role in the proper formation and orientation of axons in corticortical and corticothalamic circuits (Kostovic and Rakic, 1990; Kanold and Luhmann, 2010). Rakic likened this subplate region to a "waiting compartment" where thalamocortical axons arrive and "wait" for proper orientation (Rakic, 1976). Thalamocortical and callosal axons accumulate in the subplate before extending into the cortical plate (Kostovic and Rakic, 1990). The neurons found in this subplate are heterogeneous with regards to their morphology, the neurotransmitters used, and the neurotransmitter receptors present. This multi-faceted nature of the subplate and its neurons may be an essential part of the underlying architecture in its influence on developing axons and their incorporation into the appropriate circuits (Kostovic and Rakic, 1990). The subplate has been observed to vary in size relative to the overlying cortical plate among species, being largest in humans and primates (Aboitiz, 2007; Molnar et al., 2006). Aboitiz et al. further state that this finding suggests subplate neurons have evolved throughout mammalian history in order to support the development of complex intercortical connections that allow higher levels of cognitive processing (Aboitiz et al., 2005).

Aside from being involved with axon guidance, a subpopulation of WMNs in the adult has been associated with a possible function in vascular regulation (see discussion in Rockland and Nayyar, 2012). In the grey matter, a subpopulation of NADPH-diaphorase staining neurons has long been associated with neurovascular regulation (Cauli et al., 2004). NADPH-diaphorase is an enzyme found in a population of GABAergic neurons (Yan 1996), and co-localizes with neurons that use nitric oxide and

neuropeptide Y. Cauli et al. (2004) found that electrical stimulation of a single NOS (nitric oxide synthase) positive cortical interneuron could evoke a response in the microvasculature, including both vasodilation and vasoconstriction. It has been shown that the hemodynamic response to electrical stimulation of the basal forebrain in rodents is in part dependent on GABAergic neurons; that is, chemically inhibiting GABA-A activity resulted in a 46% decrease in cerebral blood flow following electrical stimulation when compared to a control (Kocharyan 2008). In the white matter, a subpopulation of NADPH-diaphorase neurons was shown to be in close association with several microvessels or with a single blood vessel, though the study notes that only a subset of microvessels had these associated interneurons (Rockland and Nayyar, 2012). NADPH-positive white matter neurons in the corpus callosum of transgenic mice have also been shown to have a functional role in the neuronal circuits of overlying cortex, where they have an inhibitory effect (von Engelhardt et al., 2011). Retrograde tracing experiments have further established that WMNs are incorporated into cortical circuits, though the exact function has yet to be elucidated (Tomoika and Rockland, 2007).

Counting

Cell counting has historically led to major developments in neuroscience and the current understanding of several disease states. In 1996, it was thought that neuronal loss in the hippocampus was responsible for the "benign forgetfulness" associated with old age (Wickelgren, 1996). This notion was challenged by the results of stereological analysis, which found almost no signs of neuronal loss with age in either rodents or

humans. Prior studies had focused on decreases in density, but by sampling at known intervals, investigators were able to estimate the total neuronal count, where they found minimal if any change with respect to aging (Wickelgren, 1996). Other investigations in the brains of monkeys have also reported no neuronal loss in the cortex with age (Hof et al,. 2000). Similar stereology-based studies have been performed with diseased states such as multiple sclerosis, a neurodegenerative disorder associated with autoimmune loss of the myelin sheath around axons of the central nervous system. Stereology-based studies have shown that there is significant loss of lower motor neurons in the spinal cord that can be assumed to play a role in its pathology (Vogt et al., 2009). Stereology has also been used to explore neuronal loss related to prenatal alcohol exposure, where studies found a 35% reduction in frontal cortical neurons but a 55% increase in white matter neurons in the same region (Burke, 2009).

Mortazavi et al. (2016) looked at neuronal loss in white matter in the rhesus monkey and found no loss with aging. Other studies have shown that either the distribution, density, or both of white matter neurons are affected in several disease states, including schizophrenia (Joshi et al., 2012), Alzheimer's disease (McFadden and Minshew, 2013), and even in multiple sclerosis (Chang et al., 2008) . In schizophrenia and related disorders (e.g. Bipolar disorder), subpopulations of WMNs reported to have an increased density in the superficial white matter and an altered spatial distribution, with an increased number of neurons in the deep white matter (Connor et al., 2011)

As stereology is gaining widespread use in neuroscience, it is appropriate to mention the existence of alternative techniques, such as automated cell counting and to compare its utility to manual counting, which was ultimately chosen for this study. One of the major drawbacks to stereology is its labor- and time-intensive nature. Analysis must be done manually by eye to make judgment calls on which signals should be counted according to the rules of stereology. Cells with signals that were too faint can be deemed to belong to another tissue block and thus not included in the populational count. Automatic counting would be a great boon for neuroscience research but, to date, this suffers from considerable drawbacks. In one study of automated 3D counting, Schmitz et al (2014) concluded that "stereologic cell counting with manual decision for object inclusion according to unbiased stereologic counting rules remains the only adequate method for unbiased cell quantification in histologic tissue sections." Schmitz at al. report that one of the common issues with simple automatic counting system is the failure to distinguish overlapping cells as separate entities (Figure 2).

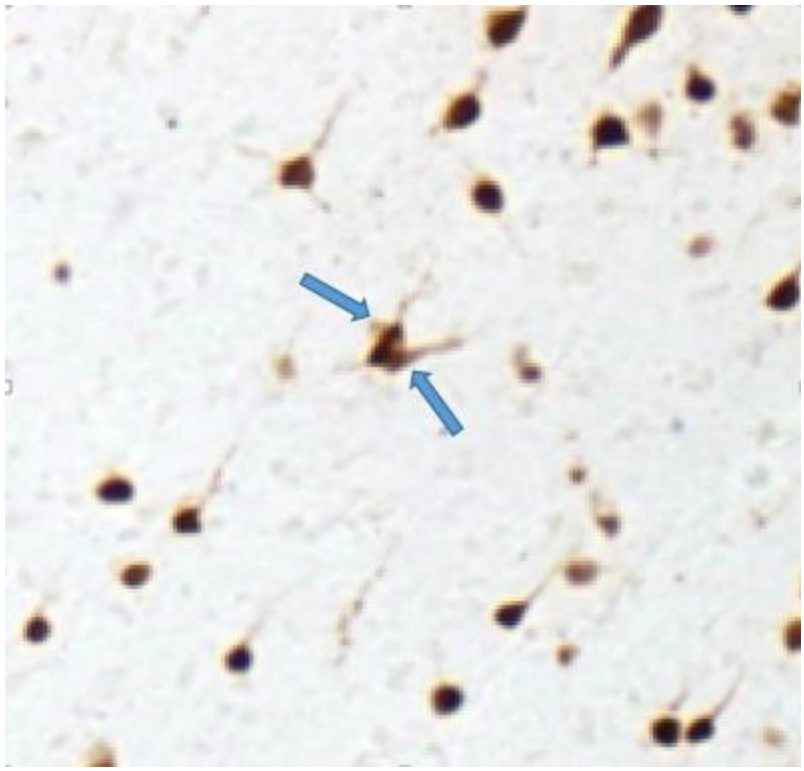

Figure 2. Example of 2 overlapping neurons that would likely be counted as one by automated stereology programs. This example was taken from the superficial white matter in the posterior parietal region. The arrows point to dendritic processes from the two separate, but overlapping neurons.

Even using the manual approach, a period of sensitization is required to recognize the more unclear cases of overlapping cells. On the other end of the complexity spectrum, Schmitz (2014) found that FARSIGHT "nuclei segmentation method" had the best results on his benchmark tests, which were comprised of a number of 3D microscopic images that were hand-counted for comparison and then run through the various automated counting routines tested. However, even FARSIGHT was found to have difficulty with certain image stacks. Schmitz (2014) reported true positive rates that ranged from 38-99% and false positive rates up to 98%. Manually entering the parameters of the algorithm helped raise the true positive rate and keep the false positive

rate low, but the results were still deemed unreliable, though the investigators did note that minimum benchmarks (such as >90% true positive, <10% false positive) could be arbitrary and could differ depending on the analysis and purpose of the study (Schmitz, 2014). As such, these investigators note that the next step in automated counting will probably be in the form of algorithms specifically designed for a particular subset of studies.

Another alternative approach to cell counting via stereology is counting via isotropic fractionator. This method was pioneered and championed by Herculano-Houzel (2015) who wrote on its comparative advantages as relates to counting with stereology. Isotropic fractionator involves dissolving the biological tissue of interest into a suspension of cell nuclei through treatment with detergents (Herculano-Houzel, 2015). After homogenizing the suspension, analysis of small aliquots can yield an estimation of the total number of cells in the biological tissue. In comparison with stereology, isotropic fractionator is a "fast and inexpensive method that requires little training, no specific software, and only a few materials" (Herculano-Houzel, 2015). The method was specifically designed to solve some of the limitations of standard stereology. One such limitations of stereology has been that the sampling parameters must be individually specialized for different structures, making gross analysis of the brain by stereology impractical (Herculano-Houzel, 2015). For example, the distribution of cells within a tissue may not be homogenous, or tissue shrinkage and artifacts resulting from the histology can affect the accuracy of such analysis. However, isotropic fractionator is not

without its own disadvantages. Because the tissue is dissolved, data about the localization of cells within the samples cannot be gathered. Herculano-Houzel (2015) puts forward a solution to this limitation by subdividing the biological tissue into regions based on function or geography, which permit modest spatial analysis. The isotropic fractionator method also provides only scant information beyond the total count in the sample. Data regarding the subtype of neurons requires further reaction with antibodies, the investigators do note, however, that tissue suspensions can be frozen for years with minimal changes in immunoreactivity (Herculano-Houzel, 2012).

The issue of counting is further complicated when stereology is applied to white matter analysis. A stereological approach requires identification of regions of interest for systematic random sampling at equidistant intervals. This analysis further depends on the borders defined. Unlike the overlying cortical grey matter, the white matter lacks, or has not yet had delineated, set structures to demarcate its boundaries. The distinction between Layer VI of the cortex and white matter is approximated by a falloff in density but is, at best, an estimation. Because there is no set threshold for cell density where grey matter ends and white matter starts, boundaries can vary from lab to lab, possibly confounding the results.

There are similar difficulties assessing where superficial white matter ends and deep white matter begins. For example, Garcia-Marin et al. (2010) defined the superficial white matter according to the convention set by Eastwood and Harrison (2003) as being immediately below the point where the white matter was "unequivocally identifiable based on the rapid decline in neuronal density from the overlying layer IV."

These investigators arbitrarily set the thickness of the superficial white matter to be 175 um and defined the deep white matter to be a 175 um thick layer, 200 um below the superficial WM. Mortazavi et al. (2016) set the superficial white matter to be 400 um; but, there is a distinct need to standardize boundaries relating to WMNs. While the current study did not examine differences in density between superficial and deep white matter, it did adopt the 400 um thick superficial white matter layer convention from Mortazavi et al.

Regional Differences

Several studies have investigated the distribution of interstitial neurons in different cortical regions. Smiley et al. counted a subpopulation of WMNs in primates and humans immuno-labelled for type m2-muscarinic receptor or histochemically labelled for acetylcholinesterase (1998). They found a decrease in cell density as they moved from immediately subjacent to the cortical grey matter towards the deeper regions. Smiley et al. also found little to no difference in density from one cortical area to another in the primate brain (1998). A similar, complementary experiment was carried out by Garcia-Marin et al (2010), which looked at the distribution and density of white matter neurons in different areas of the adult human brain. Neurons were labeled immunohistochemically with Neu-N. Obtaining results similar to Smiley et. al, Garcia-Marin found the highest density of labelled neurons to be located in the superficial white matter, with approximately four times the density of the deep white matter, as defined by the region 200 um below the superficial white matter (2010). However, Garcia-Marin et

al. (2010) did show some regional differences in the density of superficial WMNs, with frontal cortex being the densest, followed by the cingulate, visual, and finally temporal cortices. There were no regional differences found in Neu-N positive neurons of deep white matter. Another study by Mortazavi et al (2016) examined possible neuronal loss in nonhuman primates with age. The results of this study reaffirmed the greater density of white matter neurons in superficial white matter compared to deep white matter, and also found significant differences in deep white matter neuron density between frontal, temporal, and parietal regions but not in the superficial white matter.

Why Count?

Aside from being relevant to the relatively unknown functions of white matter neurons, studies on the distribution of white matter neurons may be relevant for macro imaging techniques. That is, diffusion magnetic resonance imaging (dMRI) has been used to map white matter tracts and to examine long-range anatomical connections within the cortex (Reveley. 2015). Its advantage lies in its unique ability to explore functional connectivity within the brain noninvasively by looking at the diffusion of water molecules throughout the brain. These long-range connections are axon projections that originate and terminate in the cortex but travel primarily along these white matter tracts. Reveley (2015) found that this approach resulted in a bias towards identifying tracts toward cortical gyri. They attributed this bias to "local association fibers," complex arrangements of white matter neurons in the superficial white matter that prevent communication between cortex and the deep white matter. Approximately half of the cortex was affected by this barrier,

practically limiting the viability of dMRI to detect cortical projections. The future of this technique thus necessitates development of better methods to track signals across this superficial white matter barrier. Exploring the regional distribution of white matter neurons across the brain is an obvious contributing component.

Aims

The population of white matter neurons (WMNs) has previously been reported to show regional diversity in density in relation to overlying cortical areas (Smiley et al., 1998; Garcia-Marin et al., 2010). A recent study investigating possible neuronal loss in nonhuman primates (NHP) associated with aging (Mortazavi et al., 2016) confirmed small regional differences in density but failed to show any white matter neuron loss with aging. WMNs have been broadly distinguished as superficial (immediately subjacent to layer VI) and deep (>400um below layer VI). However, further differences, in terms of gyral crown, wall, and sulcal locations have been only partly investigated (Garcia-Marin et al, 2010). Given the relevance for putative changes in density of WMNs in various pathological conditions in humans (Connors et al., 2011), we undertook a comparison in the macaque of WMN populations in a sample of cortical gyri with emphasis on standardization.

In 3 adult rhesus monkeys, WMNs were visualized by immunohistochemistry for Neu-N, which selectively labels neurons but not glia. ROIs were identified in prefrontal, temporal, and parietal cortices. Gyral WMNs were identified by exclusion of the 400um subjacent to overlying layer VI. Two approaches were used to analyze the ROIs. One was to outline the resulting territory in ImageJ, and count all neurons within this area, to derive a neuron/mm^2 number. In a complementary approach, a standardized rectangle (200um wide X 5.0mm long) was delineated at the middle of the gyrus (PFC, TE, and PP), and all NeuN-positive neurons counted within this area.

This was an effort 1) to evaluate the regional differences in neuronal density between the gyri of the prefrontal, temporal, and posterior parietal regions of three rhesus monkeys as well as 2) to explore the distribution of neurons along the gyrus from the crown towards the sulcus. It was hypothesized that this distribution would decline as we move from the region closest to the superficial white matter of the gyral crown towards the deeper white matter near sulci. While prior studies have examined regional differences in neuronal density of either superficial or deep white matter, the present study looks at the gyral white matter as a whole, and how the numbers of WMNs may vary within this.

METHODS

Tissue preparation and counting procedures were drawn heavily from Mortazavi et al. (2016).

Subjects

The tissues and images were prepared previously for use in a study by Mortazavi et al. (2016). The tissues came from 3 male rhesus monkeys (Macaca mulatta) obtained from national primate research centers. The animal identifiers and the age of the monkeys are outlined in Table 1 below. They were housed at the Laboratory Animal Science Center at Boston University Medical Center, a fully accredited institution by the Association for the Assessment and Accreditation of Laboratory Animal Care. All procedures were performed according to approved protocols and the monkeys were tested for cognitive function (Herndon et al., 1997; Moss et al., 1997; Moore et al., 2006).

Animal Identifier	Sex	Age (yr)
Am189	M	24.9
Am204	M	6.1
Am226	M	20.5

Table 1. Subject Data

Tissue Preparation and Immunohistochemistry

The monkeys were sedated (ketamine, 10 mg/kg, intramuscular) and anesthetized (sodium pentobarbital, 15 mg/kg, intravenously) prior to euthanasia (exsanguination).

The brains were perfused with 4% Krebs buffer at 4ºC and 4% paraformaldehyde in phosphate buffer (.1 M, pH 7.4) at 37ºC. The brains were then blocked in situ, removed from the skull, post-fixed in 4% paraformaldehyde and transferred into cryoprotectant. Blocks were flash frozen and stored until they were cut into coronal sections of 30 um thickness (8) and 60 um thickness (1).

The 30 micron sections from the three monkeys were thawed and rinsed 3 times for 5 minutes in .05M Tris-buffered saline. The tissue was then placed in .05M TBS with 1% hydrogen peroxide for 30 minutes and rinsed 3times for 5 minutes in .05M TBS. The tissue was transferred into a blocking solution of 10% Normal Goat Serum and .4% Triton-X in .05M TBS. The sections then were transferred to mouse anti-NeuN IgG (1:10000; MAB377, Chemicon, Temecula, CA) for 48 hours at 4ºC on a rocker. The sections were then washed 3 times for 5 minutes in .05 TBS with 2% NGS and .1% Triton-X before going into the secondary antibody (goat anti-mouse, 1:600; Vector, Burlingame, CA) in .05M TBS with 2% NGS and .4% Triton-X for 2 hours. The tissue was once again washed 3 times for 5 minutes each in .05 TBS before a final reaction in sodium acetate with .55 mM 3-3'-diaminobenzidine (DAB; Sigma, St. Louis, MO) and .01% H_2O_2 solution for 7 minutes. The sections were then rinsed for 5 minutes X 3 in .05M TBS, mounted onto subbed slides and cover-slipped.

Counting

Because there is no set structure separating superficial white matter from the subjacent layer VI, or superficial from deep white matter in rhesus monkeys, a

convention had to be established. The border between layer VI and superficial white matter was estimated on the basis of cell density and morphology, with reference to previous studies. Superficial white matter exhibits a marked decrease in both overall density of cells as well as the proportion of pyramidal cells (Figure 1). The superficial-deep WM border was established according to the conventions set in prior studies, where the initial 400 um corresponded to superficial white matter.

NeuN labeled sections were digitized using the 10x objective on an E600 Nikon microscope equipped with Turboscan Montaging system (Objective Imaging, UK). ImageJ (version 1.47, NIH, Bethesda, Md) was used to process the images and perform the counting (Figure 4). Boxes of 400x400 um were placed along the walls and crowns of gyri at the estimated border of L6/sWM. The white matter subjacent to these boxes was then enclosed using the Polygon ROI feature in ImageJ and the resulting area was called "gyral white matter" (Figure 5a). Special care was taken in areas where neurons from a tangentially sectioned layer VI could be confused as belonging in the white matter proper. Four of the total 18 sections were digitized with an alternate approach using the 4X objective on a Nikon Eclipse 80i microscope equipped with an Optronics Microfire Camera (Optronics International, USA). Images of portions of the sections were taken at 4X magnification with the software PictureFrame (Optronics International, USA). These pictures were "stitched" together to form a complete image of the gyrus using the Pairwise Stitching plugin (Preibisch et al., Bioinformatics [2009], 25([11]:1463-1465) for Fiji ImageJ (version 1.50, NIH, Bethesda, Md). To facilitate the stitching process, small

dots were placed along the cortical layers of the gyrus on the cover slip using a fine tip Sharpie marker (Figure 3). The complete image of the gyrus was then further processed by ImageJ in the same way as the other sections for rectangle analysis (Figure 5).

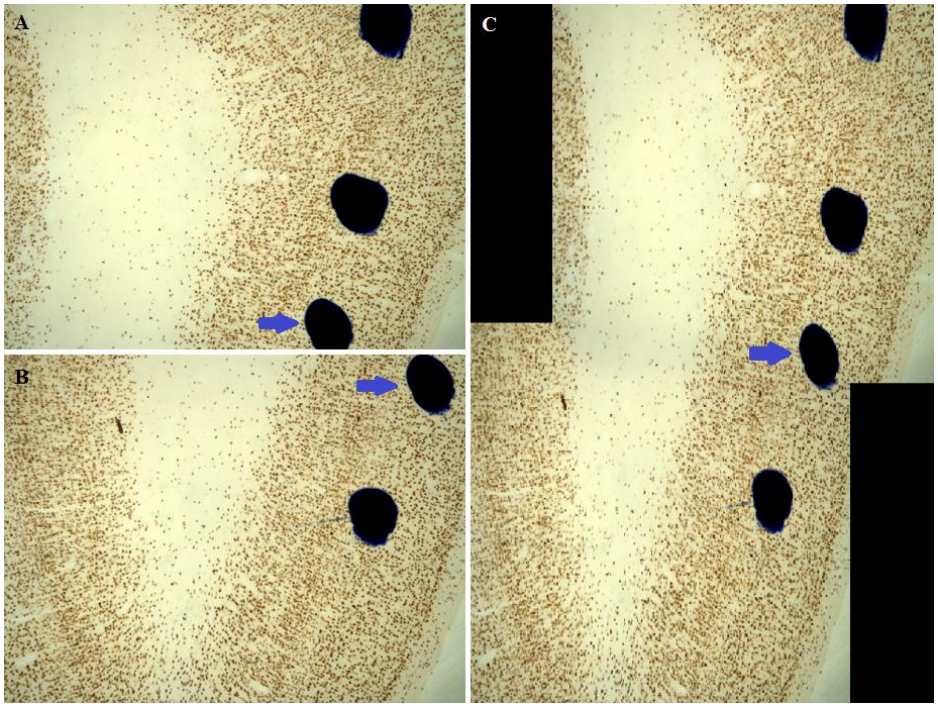

Figure 3. Example of stitching using Pairwise Stitching in Fiji ImageJ. Pictures in (a) and (b) were combined to form the image shown in (c). The blue arrows point to the Sharpie dot overlap. The black regions on the top left and bottom right of (c) are the result of horizontal translation during stitching.

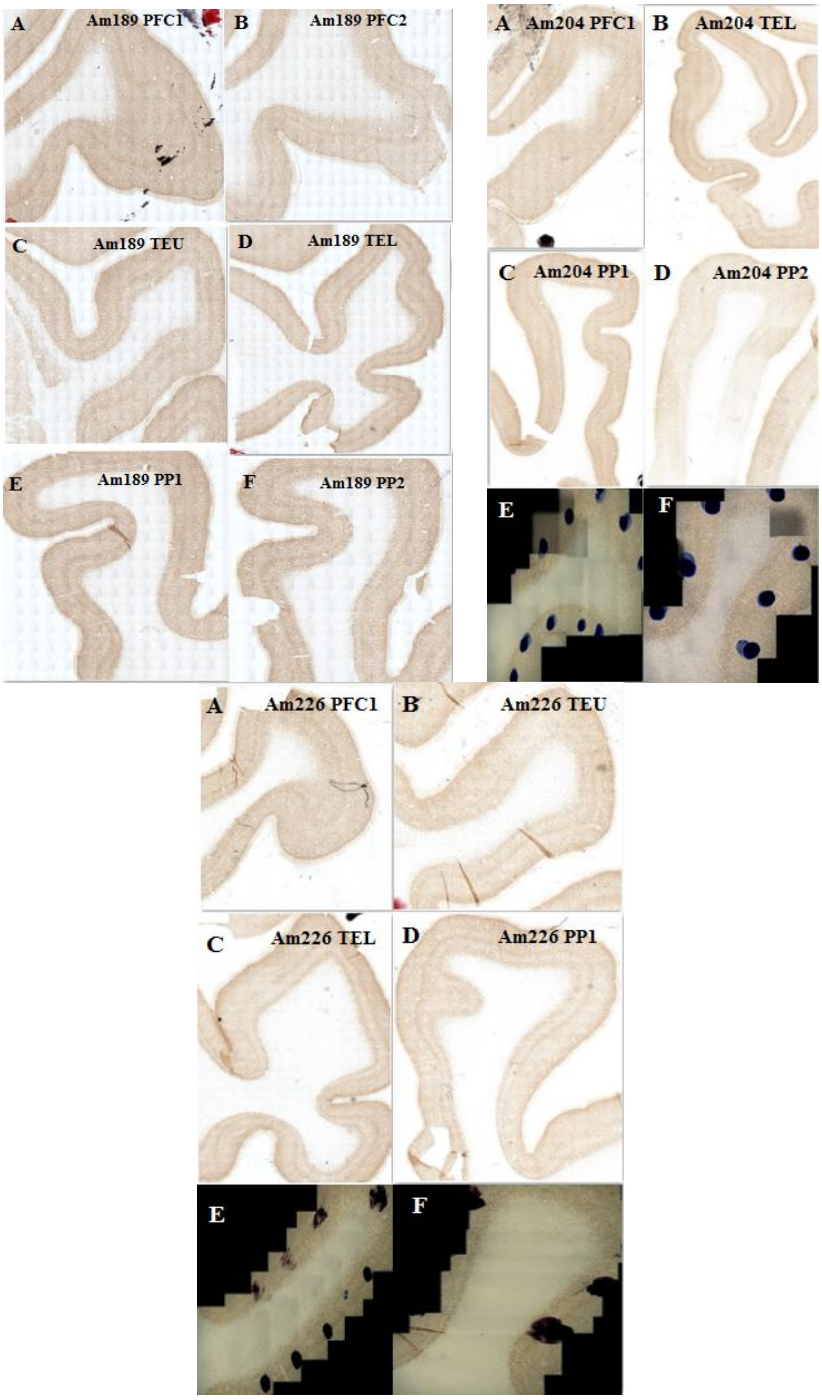

Figure 4. Condensed mosaic image of the digitized sections. Animal identifiers are noted above the image and individual sections are labeled from A-F. Am204 and Am226 E and F were the product of the pairwise stitching process using Fiji.

To estimate cell density, the area of the polygon ROI was determined with the ImageJ Measure function. Using ImageJ's cell counter, neurons within the polygon ROI were marked to provide a total count. Density was estimated by dividing the total neuronal count by the area of the sampling region to calculate neuron/mm^2. As a complementary approach, a 200x5000 um rectangle was placed along the long axis of the gyri (Figure 5b). The rectangle was then divided into 4 smaller, equivalent 200x1250 um regions to investigate fall-off in cell density. If placing a single 200x5000 um rectangle proved difficult, 4 200x1250 um rectangles were angled and laid end-to-end to best simulate the original approach (Figure 5c). A second double-check for cell density was performed by an impartial experimenter by superimposing a 400x400 grid onto the images. Only grid boxes fully inside the gyral white matter ROI were used in this approach. One in three boxes were sampled and the total cell count was estimated by taking the average number of neurons counted per box and multiplying by a correcting factor (Total Area of ROI divided by Area of Sample Box). This approach was taken to approximate a stereological approach to counting. In the aforementioned four samples taken by a 4x objective (40X magnification), only the rectangle approach was taken due to time constraints.

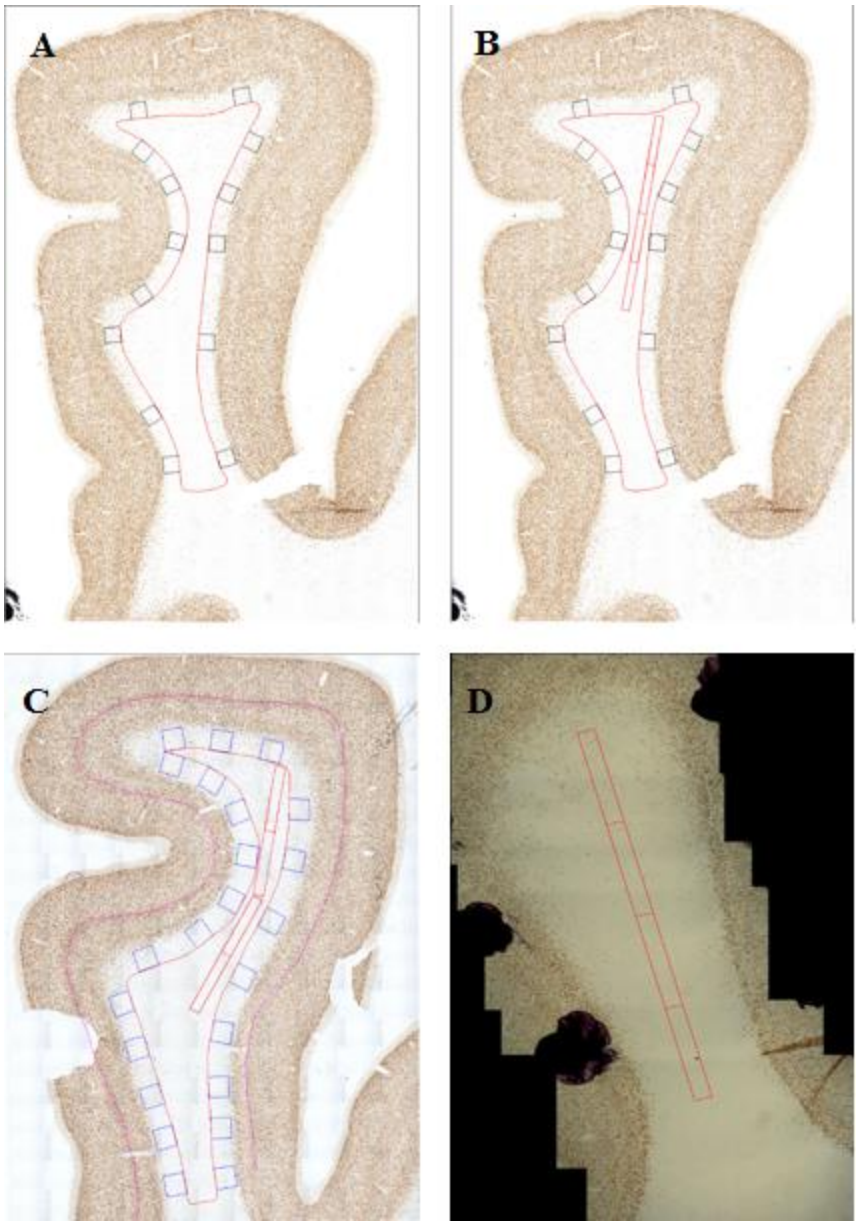

Figure 5. (a) Posterior parietal (PP) section from Am204 showing the boxes placed along the edge of the superficial white matter and the enclosed gyral white matter. (b) The same figure in (a) with the 200um x 5000um added and subdivisions shown. (c) A similar PP section from Am189 showing a situation where rectangle subsections were broken and laid end to end. (d) A PP section from Am226 that was digitized separately. Rectangle analysis was performed but the gyral white matter was not sampled otherwise.

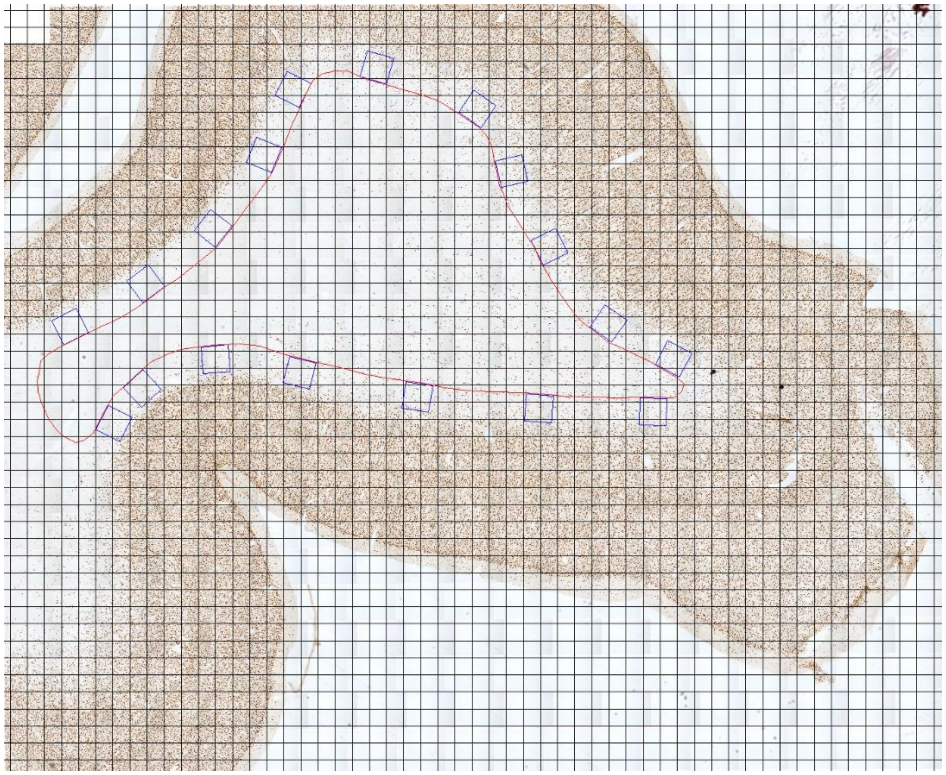

Figure 6. A PFC section from Am189 showing the overlaid counting grid. Only Boxes fully enclosed in the outlined gyral white matter were sampled, with the intent of performing a double check of the manual counts.

Statistical Analysis

Due to the small sample size of the data gathered, non-parametric tests were used to analyze the density of white matter neuron distribution across the different cortical regions of the brain and across the four zones in each region sampled. Parametric statistics were also performed in certain cases just for explorative purposes. All but one of the statistics were performed using the software Statistical Package for Social Sciences (SPSS, version 23.0, Chicago, Ill., USA). Unless otherwise stated, results are given as mean$\pm$SEM and alpha was set at 0.05.

RESULTS

Choice of cortical regions

To study the differences in regional density of WMNs, we sampled three rhesus monkey brains with six ROI identified per animal (Table 2). For each animal, two ROIs were determined for each region (frontal, temporal, and parietal). White matter was historically thought to be passive tissue, with cortico-cortical circuits passing through in bundles of fibers. As the known functions of white matter neurons are more integrative rather than sensory, the ROIs for this study were identified from association rather than primary cortex. The regions selected also represent diverse sampling along the anterior-posterior axis. Initially, the temporal sections were treated and analyzed as one coherent region of the brain but the different overall morphological structure and the data gathered suggested that the area below and above the Superior Temporal Sulcus (STS) was best treated as two distinct areas.

	Animals	**Sample per Animal**	**Total ROIs**
Prefrontal	3	2	6
Temporal above STS	3	1	3
Temporal below STS	3	1	3
Posterior Parietal	3	2	6

Table 2. Number of Samples

Regional Density

Using ImageJ's Cell Count function, total counts of gyral white matter neurons were obtained in 14 out of the 18 ROI studied. The sampled data include four ROIs in prefrontal cortex, two ROIs in the temporal cortex above the superior temporal sulcus,

three ROIs in the temporal cortex below the STS, and five ROIs in the posterior parietal sulcus. Because the results from the temporal cortex below and above the superior temporal sulcus were so different, the two were treated as different regions. Because the size of the gyrus and therefore the ROI from section to section could vary, white matter neuron density was normalized to neurons per millimeter squared to better enable comparison. The density for each region was calculated by taking the total neuronal counts (neurons) and dividing by the area of the ROI sampled (mm^2). Table 3 below summarizes the data.

Region	**Density (neurons/mm^2)**
Am189 PFC1	162.49
Am189 PFC2	239.78
Am204 PFC1	247.61
Am226 PFC1	338.17
AVG	*247.01±35.95*
Am189 TEU	282.69
Am226 TEU	416.19
AVG	*349.44±66.75*
Am189 TEL	114.15
Am204 TEL	165.14
Am226 TEL	161.64
AVG	*146.98±16.44*
Am189 PP1	64.70
Am189 PP2	58.32
Am204 PP1	133.50
Am204 PP2	180.10
Am226 PP1	94.95
AVG	*106.31±22.75*

Table 3. Regional counting

In each of the regions sampled, subject Am189 was consistently the least dense. There was no set pattern regarding Am204 and Am226. Discounting the temporal region above the STS (TEU in Table 3), the prefrontal cortex was the most dense, followed by the temporal region below the STS (TEL in Table 3), and finally the posterior parietal. This data is graphically represented in Figure 7.

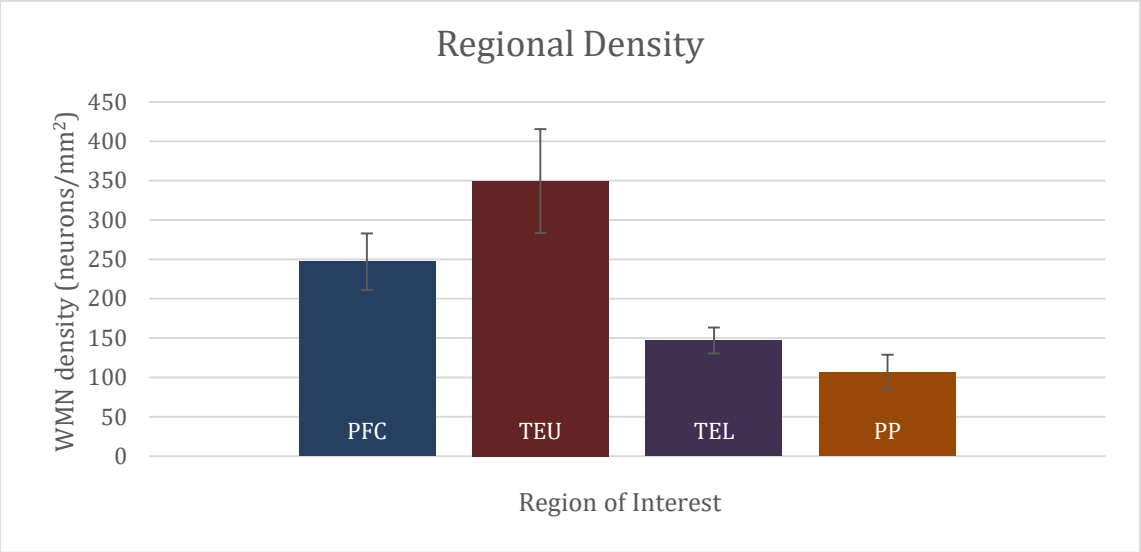

Figure 7. White matter neuron densities are averaged across the samples taken and reported along with the standard errors of the mean.

Statistical analysis

Because of missing data points and the resulting varying sample size between regions, analysis of the data from different regions was performed with the Skillings Mack test package (a variation Friedman's designed to be used with missing data) [Patchanok Srisuradetchai (2015). Skillings.Mack: The Skillings-Mack Test Statistic for Block Designs with Missing Observations. R package version 1.10.] in the statistical software R (R Core Team (2016). R: A language and environment for statistical

computing. R Foundation for Statistical Computing, Vienna, Austria. R version 3.24). Data gathered from the TEU sections were omitted from this analysis. The Skillings Mack test found a non-significant difference in density between the three sampled regions (Skilling-Mack Statistics = 6.38, p = .17).

For the purposes of future study, all of the data regarding densities in individual regions, including the data from TEU omitted from the previous analysis, were also processed with a one-way ANOVA test. For this test, the Shapiro-Wilks test was used to determine whether the data obtained fit a normal distribution. While the TEU data couldn't be tested in this manner due to its small sample size, the test determined that the data from the other three regions did fit a normal distribution. For the purposes of this analysis, we assumed a normal distribution for the TEU as well, simply to get an idea of what the results may have been. The results are outlined in Table 4. Though, as noted, this was not the most appropriate statistics for the data set, ANOVA analysis showed a statistically significant difference in white matter neuron density between the groups, particularly between PFC and PP (p = .025), TEU and TEL (p = .019), and TEU and PP (p = .003).

Comparison	F value	Significance
Between Groups (Overall)	9.565	.003
PFC and TEU		.265
PFC and TEL		.196
PFC and PP		.026
TEU and TEL		.019
TEU and PP		.003
TEL and PP		.794

Table 4. Results of the One-Way ANOVA and post-hoc Tukey HSD test. There was an overall statistically significant difference as well as differences between three pairs of regions.

Grid double check

An approach that approximated stereology was used in order to double check the raw counts. Estimated cell counts were calculated from the counts sampled in an overlaid 400x400 um grid and are outlined in Table 5 along with the percent error for each of the sampled ROI as compared to counts found by hand in ImageJ.

Region	Raw Count	Grid Estimation	% Error
Am189 PFC1	393	254.95	-35.38
Am189 PFC2	2617	2143.87	-18.08
Am204 PFC1	661	704.93	+6.65
Am226 PFC1	365	400.26	+9.66
Am189 TEU	1058	921.62	-12.89
Am226 TEU	1118	1121.51	+.31
Am189 TEL	892	704.97	-20.97
Am204 TEL	1234	1133.05	-8.18
Am226 TEL	2437	1586.83	-34.89
Am189 PP1	547	446.75	-18.33
Am189 PP2	240	324.88	+35.37
Am204 PP1	861	1017.02	+18.12
Am204 PP2	565	437.06	-22.64
Am226 PP1	584	375.23	-35.75

Table 5. Grid double check

The grid estimation tended to underestimate the neuronal counts, with 9 out of the 14 sampled areas containing more neurons in the actual count than estimated. Of the six Am189 ROIs sampled, all but one of the parietal association areas had a greater total count than estimated by the grid convention. The other two subjects, Am204 and Am226 each had 2 underestimated and two overestimated counts. The temporal section below the STS (TEL) was the only region that was underestimated each time by the grid double check.

Rectangle Analysis

Another metric was to take counts within a 200x5000 um rectangle divided into four equivalent zones of 200x1250 um superimposed along the gyral white matter. All 18 ROIs were sampled in this manner. Table 6 below summarizes the findings of white matter densities in each zone along the gyrus, with Zone 1 corresponding to the 200x1250 um rectangle closest to the gyral crown and Zone 4 corresponding to rectangle furthest from the crown. The average neuronal density of the entire 200x5000 um rectangle is also given.

		Zone 1 (neu/mm^2)	Zone 2 (neu/mm^2)	Zone 3 (neu/mm^2)	Zone 4 (neu/mm^2)	*Average (neu/mm^2)*
PFC	Am189-1	84	32	20	36	*43*
	Am189-2	144	76	36	32	*72*
	Am204-1	96	84	44	44	*67*
	Am204-2	176	96	80	64	*104*
	Am226-1	260	60	40	28	*97*
	Am226-2	172	92	60	52	*94*
TEU	Am189-1	172	64	72	80	*97*
	Am204-1	292	104	124	208	*182*
	Am226-1	220	176	192	192	*195*
TEL	Am189-1	68	24	24	24	*35*
	Am204-1	56	36	32	48	*43*
	Am226-1	164	52	28	16	*65*
PP	Am189-1	32	28	12	8	*20*
	Am189-2	48	16	16	8	*22*
	Am204-1	120	88	28	28	*66*
	Am204-2	172	44	32	56	*76*
	Am226-1	128	40	8	24	*50*
	Am226-2	28	16	16	12	*18*

Table 6. White matter neuron density as found in the four 200x1250 um rectangles with the average density of the entire 200x5000 um rectangle given.

All rectangles analyzed had some, if minimal, drop-off in density moving from Zone 1 to Zone 2. This trend continued in Zone 3 in all but the 3 TEU regions, which notably all had increases in density past Zone 2. This corresponded with a narrowing of the gyri towards the later zones, which may have caused increased sampling of neurons closer to superficial white matter. 7 of the 18 ROIs sampled also saw increases from Zone 3 to Zone 4, including all 3 TEU samples. The data in Table 6 is graphically represented in Figure 8.

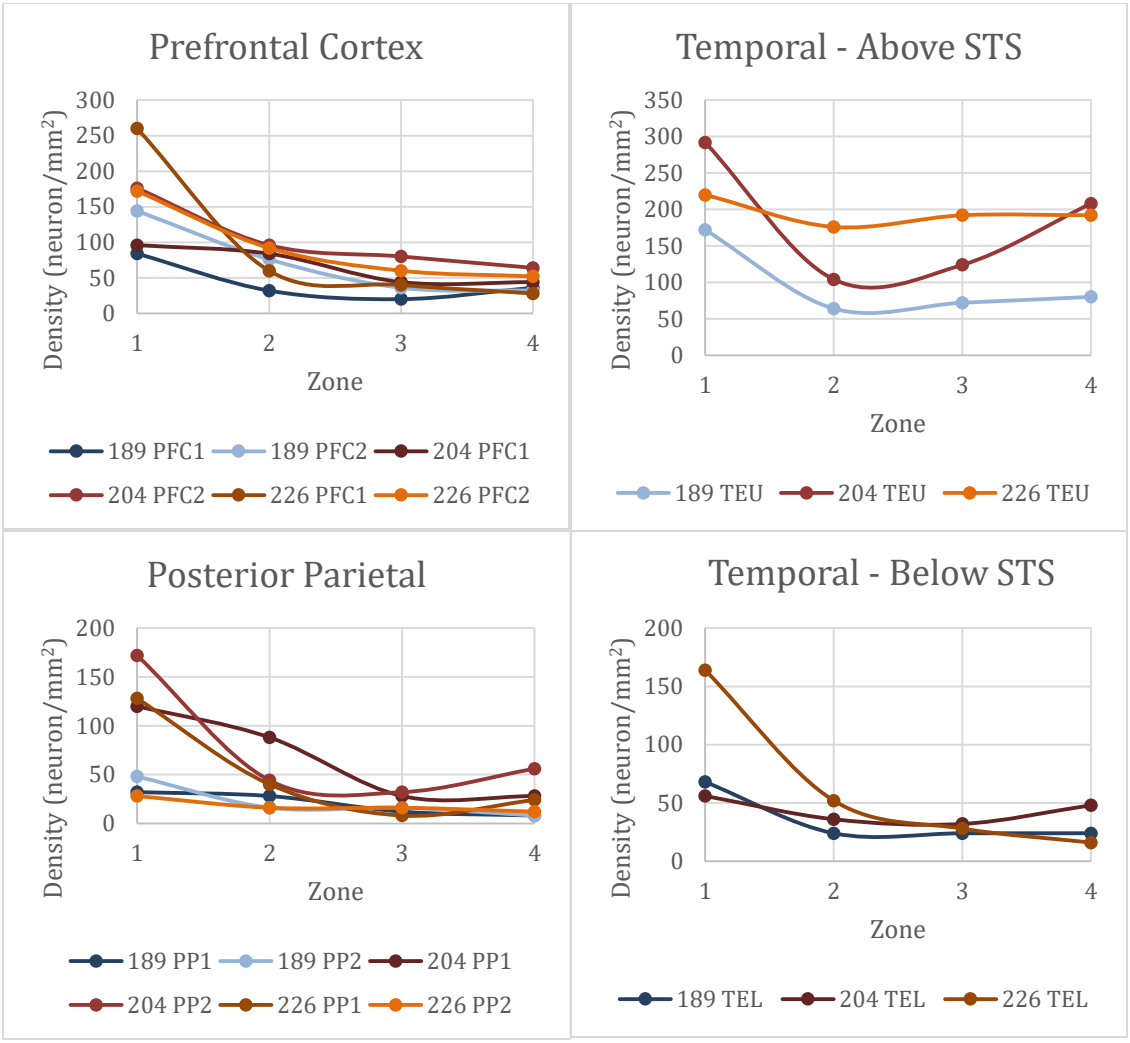

Figure 8. Graph of the pattern of average white matter neuron densities in the four ROIs moving from Zone 1 to Zone 4. Zone 1 was defined as the 200um x 1250um rectangle closest to the crown of the gyrus and Zone 4 the 200um x 1250um rectangle furthest from the crown.

To analyze the fall-off of white matter neuron density across zones moving from the crown of the gyrus to deeper white matter, the data from samples from each region were pooled. Select comparisons of neuronal density between zones in each region can be seen in Table 7.

	Z1 vs. Z2	Z1 vs. Z4	Z2 vs. Z3	Z2 vs. Z4	Z3 vs. Z4
PFC	-52.8%	-72.5%	-36.4%	-41.8%	-8.57%
TEU	-49.7%	-29.8%	+12.8%	+39.5%	+23.7%
TEL	-61.1%	-69.4%	-25.0%	-21.4%	+4.75%
PP	-56.1%	-75.2%	-51.7%	-41.3%	+21.4%

Table 7. Selected comparisons of neuronal density between zones amongst the pooled data as a measure of percentage change.

Of the twenty comparisons shown in Table 7, all but five were decreases in neuronal density moving away from the crown of the gyrus. All four regions had an overall decrease in density as measured by Z1 vs. Z4 comparisons. The PFC, TEL, and PP regions had greater density decreases in the Z1/Z4 comparison than they did in the Z1/Z2; however the TEU, as previously noted, has increased density moving from Z2-Z3 and Z3-Z4.

Statistical analysis

A Friedman's test showed statistically significant differences in densities of WMNs across the four different zones in three of the four regions (PFC, TEU, PP, but not TEL) [Table 8].

Region	χ^2	df	p value
PFC	15	3	.002
TEU	8.793	3	.032
TEL	6.692	3	.082
PP	13.947	3	.003

Table 8. Results of Friedman's Test. The PFC, TEU, and PP all showed significant differences in WMN density across zones ($p < .05$), but the TEL did not ($p > .05$).

Region	Zone 1	Zone 2	Zone 3	Zone 4
PFC	4	2.83	1.75	1.42
TEU	4	1	2.17	2.83
TEL	4	2.33	1.67	2
PP	4	2.67	1.75	1.58

Table 9. Friedman's Test Ranks Results. This table shows the ranks of the different zones across each region as calculated with the Friedman's test. Only the PFC and the PP showed the hypothesized decrease in rankings moving to subsequent zones.

While the Friedman's test reported differences between zones, only the PFC and PP regions showed the expected consistent decrease in density rank moving from Zone 1 to Zone 4 (Table 9). The density ranks for TEU decreased from Zone 1 to Zone 2, but then started to increase from Zone 2 to 3 and even to Zone 4. The TEL also exhibited decreased density moving from Zone 1 to Zones 2 and 3 but increased moving to Zone 4. Moreover, post-hoc analysis using the Wilcoxon signed-rank test with Bonferroni correction for multiple analysis failed to show a statistically significant fall-off in adjacent zones in every case ($p > .0083$, Table 10).

Region	Z1-Z2	Z2-Z3	Z3-Z4
PFC	$p = .027$	$p = .027$	$p = .416$
TEU	$p = .109$	$p = .109$	$p = .180$
PP	$p = .027$	$p = .068$	$p = .684$

Table 10. Selected results from Wilcoxon signed-rank test. With Bonferroni correction, p values must be less than .0083 to be statistically significant.

DISCUSSION

Purpose

This study was performed to quantitatively explore regional differences in white matter neuron density in the rhesus monkey. In order to do so, we sampled gyral white matter from three association areas: the prefrontal cortex, temporal cortex, and posterior parietal cortex. Association areas were chosen due to its close historical ties with white matter. The nerve fibers connecting different cortical areas to each other have been shown to travel through the white matter, a preeminent example being the corpus callosum. As such, association areas made a better candidate than primary cortex in an investigation of white matter neurons. These three areas were also chosen for their spatial configuration, as they represent differing positions anteriorly/posteriorly and laterally within the brain. To date, only a few of the functions of white matter neurons and the circuits they participate in have been investigated. White matter and its distribution have, however, been implicated in several pathologies, including epilepsy, schizophrenia, multiple sclerosis, and even Alzheimer's disease. Its distribution also has important implications in diffusion magnetic resonance imaging, which uses the diffusion of water through the brain to track long-range connections. Detailed anatomical mapping obtained through diffusion MRI has had important clinical applications, including surgery (Kleisser 2009). However, barriers formed by local association fibers in the superficial white matter limit detection of cortical connections.

Early attempts and pitfalls

To investigate the differential distribution of white matter neurons in the PFC, TE, and PP regions, we outlined a region of interest that we termed the gyral white matter as outlined by the area within the white matter excluding the most superficial 400um. As previously mentioned, there is no set structure delineating the border between cortical Layer VI and the white matter. As such, the borders drawn were approximated by visually inspecting the decrease in cellular density and can vary somewhat from section to section and even within sections. The initial direction of the study was to take total counts from this gyral white matter and compare them across the different regions. To further look at drop-off moving along the length of the gyrus, we had initially separated the gyral white matter into approximately equivalent subsections which also served the secondary function of making the task of total counting more manageable (see Figure 9 below).

Figure 9. Example of initial analysis method of a section from the Temporal lobe above the superior temporal sulcus. The gyrus is divided into approximately equal subsections to be sampled individually.

However, this method was not optimal for standardizing the subdivisions across gyri that had vastly different shapes and area measurements. To address the latter issue, we adopted a standardized metric, neurons per square millimeter, but found that the former issue remained. As an attempt to further standardize, analysis via rectangles was adopted. The Rectangle Analysis approach to studying WMN distribution in the gyral white matter provides a quick, innovative method to gather data. It is a robust metric as it can be easily adapted to different gyri. Because the rectangles are superimposed along

the center of the gyri, it avoids certain confounding factors such as tangentially-cut cortical layers being misinterpreted as superficial white matter. Moreover, as the individual zones can be counted separately and angled if necessary, gyri that aren't necessarily completely straight can also be analyzed using this method. Since the measurements are taken in terms of neuronal density, the rectangle width can be modified to fit sections of varying thickness, and the length can be modified by adding or removing additional zones. In the current study, the rectangles used were standardized as 200um wide and 5000um long split into four 200x1250um "zones."

There was also an issue applying the gyral white matter polygon to the four sections obtained via Fiji image stitching. In these sections, placement of the 400x400 um boxes left insufficient space within which to circumscribe our polygon. As such, these sections were omitted from the total density counts and only analyzed using the rectangle method, with placement of counting rectangles closest to the center.

Another pitfall of the current study was the difficulty in assessing whether particularly faint staining signals should be counted or not. Signals that were too faint to readily discern could have been neurons from a different layer that shouldn't be sampled. There were also size discrepancies between neurons as well, probably due to the position of the neuron relative to the plane of cutting. While the digitized slides made counting simpler, being unable to physically examine the slides under a microscope and change focus made interpreting the fringe cases difficult. These distinctions was further confounded by the initial conversion of digitized images to black and white due to the large file size of the original images. In the black and white images, specks of dirt on the

slide could sometimes be mistaken for neurons and thus muddle the count. The images were recounted in color for the purposes of this study. Neuronal signals that were too faint were also omitted from the counts, though this distinction was left to the particular researcher's discretion.

Results and statistical analysis

From the previous literature, the expected results were a decrease in white matter neuron density in the deep white matter when compared to that in the superficial white matter. This trend was further applied to the rectangle analysis performed in this study. Specific expectations were 1) that moving from the crown deeper into the gyrus would systematically result in decreasing neuron density and 2), there would be regional differences. The current study of white matter neuron distribution in NHP had in actuality mixed results. While there was a statistically significant difference both between the different zones in the rectangular analysis and between different overlying cortical areas, post-hoc analysis failed to show significant differences across specific regions. This discrepancy with expectation may be due to the small sample size of this study as well as to the inherently conservative nature of the Bonferroni correction for multiple analysis, which have much stricter requirements for statistical significance. Thus, it proved difficult to draw conclusions with appropriate confidence levels from the data obtained.

It is noted that both the chi-squared test statistic and confidence interval obtained is much higher for the prefrontal cortex and posterior parietal cortex, which had six

samples each when compared to the temporal sections, which had three samples apiece. As such, studies with larger sample sizes may obtain more conclusive results. Initial expectations were that neuronal density would decrease moving from Zone 1 to each subsequent zone. The Friedman test for PFC and PP showed the hypothesized decreases in rank but the tests for the temporal sections did not align with the projected results. In the TEU and TEL, there was an overall decrease in density between Zones 1 and 2 and Zones 1 and 4, but there were unexpected increases in the Z3-4 transition for both above and below the STS and in the Z2-3 transition for the TEU (see Table 7). Similar increases between Z3-4 were also noticed in some sections of the un-pooled data from PFC and PP sections. Though the post-hoc Wilcoxon signed-ranked test showed that the results did not attain significance, our raw data do corroborate a decrease moving from Zone 1 to 4. As Zone 1 is the sampled region closest to the superficial WM at the crown of the gyrus, its high density of WMNs matches expectations. In certain sections, however, the sampling rectangles for Zones 3 and 4 coincide with a narrowing of the gyrus. One such section, Am189 TEU, is reproduced in Figure 10, with the corresponding neuron density counts from Table 6 also provided. As the gyrus narrows, the rectangle samples closer to the denser superficial white matter, at times possibly even sampling tangentially sectioned cortical neurons, resulting in higher neuronal density in Zones 3 and 4 (Figure 10).

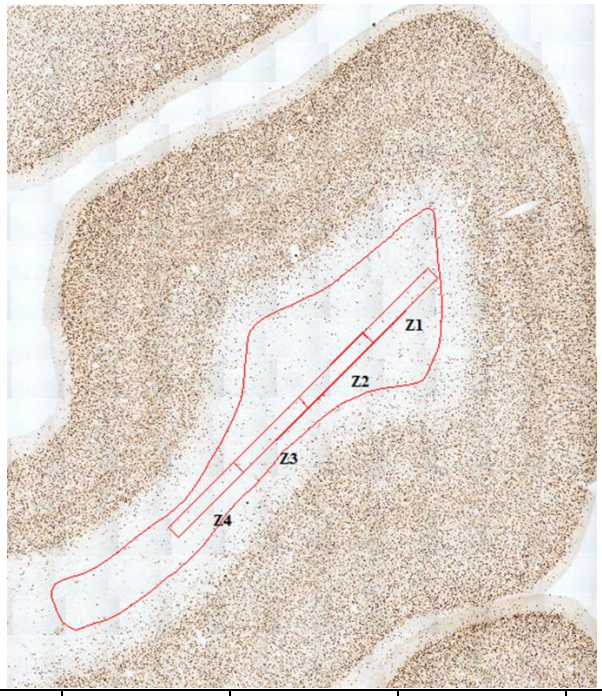

		Zone 1 (neu/mm^2)	Zone 2 (neu/mm^2)	Zone 3 (neu/mm^2)	Zone 4 (neu/mm^2)
TEU	Am189-1	172	64	72	80

Figure 10. Rectangle analysis performed on Am189 TEU. Note that as the gyrus widens, the boxes necessarily sample closer to the edges of the polygon, closer to the denser superficial white matter. The appropriate portion of Table 6 is also reproduced.

Previous studies attempting to quantify white matter neuron density have reported regional differences to varying extents. Garcia-Marin et al reported, in postmortem human brain, a four-fold difference in superficial white matter neurons compared to deep matter neurons and some regional differences in superficial white matter neurons across the brain (Garcia-Marin 2010). Smiley et al (2010) found a similar difference in density between superficial and deep white matter but failed to observe regional variations in monkey except in a medial section of primary visual sulcus. Mortazavi (2016) also obtained results indicating a significant decrease in white matter neurons moving from superficial to deeper white matter as well as a lower density in the temporal region

compared to frontal or cingulate cortex. Because the procedures for visualizing neurons and counting, including ROI selection, are different from lab to lab, the variation in results is unsurprising.

A major limitation of the current study was the small sample sizes in each region. While our results failed to show a statistically significant difference in the density of white matter neurons across the three regions of the brain, the raw numbers were more suggestive. With a larger sample size, the differences between the regions may become more convincing as statistical outliers may be averaged out. While the Skillings-Mack test was the most appropriate test for such a data set with several missing entries, an alternative test via 1-way ANOVA provided more promising results. When all data points were analyzed, the ANOVA found a statistically significant difference across different regions, with post-hoc Tukey HSD tests showing the most notable differences in density occurred between the PFC-PP, TEU-TEL, and TEU-PP regions.

Future directions

Directions for future study include obtaining data from a larger sample of animals and regions using the rectangle analysis as well as the overall gyral counts. As previously discussed, the data seemed to support a trend but confidence levels were low due to the small sample size. With a larger sample size, we hope to minimize the effect of outliers from the collected data and form a more cohesive picture. Another direction could be sampling directly from the superficial white matter in the wall of the gyrus to see whether a similar pattern exists. Boxes placed on the digitized images in order to

outline the gyral white matter are a good area of focus. While the rectangle analysis is helpful, it by design moves the sampling area closer to deeper white matter where neuronal density is expected to decrease. As such, it is unclear whether any downward trends in white matter neuron density would be due to position along the length of the gyrus or due to the movement of sampling region from superficial to deeper white matter. By sampling the 400 um white matter immediately subjacent to overlying cortical areas, we can avoid the confounding effects that differences in position along the white matter makes and more coherently study trends along a gyrus.

Further areas of research include:

1. sampling from the sulci adjacent to the gyri to explore further regional differences among animals
2. analyzing differences in density between the gyral crown, wall, and adjacent sulci
3. using stains for GABAergic neurons to assess whether fall-off in neuronal density across zones is more pronounced in inhibitory or excitatory subpopulations of white matter neurons.

Since many of the previous studies such as Garcia-Marin (2010) and Smiley et al (1998) have sampled from the walls of the gyri, comparison with the sulcal areas is a relatively unexplored direction.

A possible advance for neuronal counting exists in the form of 3-D counting. Previously mentioned was the importance of establishing a standardized convention for the boundaries in white matter. Of note are the cases where the width of the gyrus could

not accommodate both the 400x400 um demarcation boxes and a gyral white matter polygon. This raises the question of what to do in cases where the gyrus being analyzed is too narrow to adhere to sampling conventions. Is it possible that there are gyral sections with no "deep white matter" and only superficial white matter? However, counting using 3-D slabs of roughly 200-300 um thick provides a possible solution to this issue. 3-D imaging alleviates the issue with 2-D imaging and fringe cases, allowing more accurate counts. It also offers areas for further study such as three dimensional morphometric analysis of neurons similar to that done by Mortazavi et al (2016).

Conclusion

This study was started to examine differences in white matter neuron density across animals both between and within association areas of the brain. The results were promising but lack of sufficient sample size made drawing conclusions with confidence difficult. Nevertheless, the general trend of decreasing neuronal density moving from the crown of the gyrus away is present in most sections examined. Potential areas of further study include the neuronal distributions along the wall rather than the center of gyri and adjacent sulci along with morphometric analysis of neurons such as those performed by Mortazavi et al. Such information may prove instrumental in the study and clinical treatment of pathologies such as Alzheimer's disease, epilepsy, schizophrenia and related disorders or even normal bodily functions like sleep (Kulduff et al., 2011) and vascular regulation.

REFERENCES

Aboitiz, F., Montiel, J., & García, R. R. (2005). Ancestry of the Mammalian Preplate and its Derivatives: Evolutionary Relicts or Embryonic Adaptations? Reviews in the Neurosciences, 16(4).

Aboitiz F, Montiel J. 2007. Origin and evolution of the vertebrate telencephalon, with special reference to the mammalian neocortex. Advances in Anatomy, Embryology and Cell Biology, 193:1–112

Burke, M. W., Palmour, R. M., Ervin, F. R., & Ptito, M. (2009). Neuronal reduction in frontal cortex of primates after prenatal alcohol exposure. *NeuroReport, 20*(1), 13-17. doi:10.1097/wnr.0b013e32831b449c

Cauli B., Tong X. K., Rancillac A., Serluca N., Lambolez B., Rossier J., Hamel E. (2004). Cortical GABA interneurons in neurovascular coupling: relays for subcortical vasoactive pathways. Journal of Neuroscience. 24, 8940–894910.1523/JNEUROSCI.3065-04.2004

Chang, A., Smith, M. C., Yin, X. Fox, R. J., Staugaitis, S. M., and Trapp, B. D. (2008). Neurogenesis in the chronic lesions of multiple sclerosis. Brain, 2366-2375. doi: 10.1093/brain/awn157

Connor, C. M., Crawford, B. C., & Akbarian, S. (2011). White Matter Neuron Alterations in Schizophrenia and Related Disorders. *International Journal of Developmental Neuroscience : The Official Journal of the International Society for Developmental Neuroscience*, *29*(3), 325–334. http://doi.org/10.1016/j.ijdevneu.2010.07.236

Eastwood SL, Harrison PJ. 2003. Interstitial white matter neurons express less reelin and are abnormally distributed in schizophrenia: toward an integration of molecular and morphologic aspects of the neurodevelopmental hypothesis. Molecular Psychiatry 8:769, 821–831.

García-Marin, V., Blazquez-Llorca, L., Rodriguez, J. R., Gonzalez-Soriano, J., and DeFelipe, J. (2010). Differential distribution of neurons in the gyral white matter of the human cerebral cortex. *Journal of Comparative Neurology* 518, 4740-4759. doi: 10.1002/cne.22485

Herculano-Houzel S. The isotropic fractionator: a fast, reliable method to determine numbers of cells in the brain or other tissues. In: Fellin T, Halassa MM, editors. Springer Neuromethods: Neuronal network analysis: concepts and experimental approaches. Vol. 67. Humana Press; New York: 2012. pp. 391–403.

Herculano-Houzel, S., von Bartheld, C. S., Miller, D. J., & Kaas, J. (2015). How to count cells: the advantages and disadvantages of the isotropic fractionator compared with stereology. Cell and Tissue Research, 360(1), 29–42. http://doi.org.ezproxy.bu.edu/10.1007/s00441-015-2127-6

Hof, P. R., Nimchinsky, E. A., Young, W. G., and Morrison, J. H. (2000). Numbers of meynert and layer IVB cells in area V1: a stereologic analysis in young and aged macaque monkeys. Journal of Comparative Neurology, 113-126. doi: 10.1002/(SICI)1096- 9861(20000424)420:1<113::AID-CNE8>3.0.CO;2-N

Joshi, D., Fung, S. J., Rothwell, A., and Weickert, C. S. (2012). Higher gamma-aminobutyric acid neuron density in the white matter of orbital frontal cortex in schizophrenia. Biological Psychiatry 72, 725-733. doi: 10.1016/j.biopsych.2012.06.021

Judaš, M., Sedmak, G., & Pletikos, M. (2010). Early history of subplate and interstitial neurons: From Theodor Meynert (1867) to the discovery of the subplate zone (1974). *Journal of Anatomy*, *217*(4), 344-367.

Kanold, P. O., & Luhmann, H. J. (2010). The Subplate and Early Cortical Circuits. Annu. Rev. Neurosci. Annual Review of Neuroscience, 33(1), 23-48.

Kilduff, T. S., Cauli, B., & Gerashchenko, D. (2011). Activation of Cortical Interneurons During Sleep: An Anatomical Link to Homeostatic Sleep Regulation? *Trends in Neurosciences*, *34*(1), 10–19. http://doi.org/10.1016/j.tins.2010.09.005

Kleiser, Raimund, Philipp Staempfli, Anton Valavanis, Peter Boesiger, and Spyros Kollias. "Impact of FMRI-guided Advanced DTI Fiber Tracking Techniques on Their Clinical Applications in Patients with Brain Tumors." Neuroradiology 52.1 (2009): 37-46. Web

Kocharyan A., Fernandes P., Tong X. K., Vaucher E., Hamel E. (2008). Specific subtypes of cortical GABA interneurons contribute to the neurovascular coupling response to basal forebrain stimulation. Journal of Cerebral Blood Flow and Metabolism. 28, 221– 23110.1038/sj.jcbfm.9600558

Kostovic I, Rakic P. Cytology and time of origin of interstitial neurons in the white matter in infant and adult human and monkey telencephalon. Journal of Neurocytology. 1980;9:219–242.

Kostovic I, Rakic P (1990) Developmental history of the transient subplate zone in the visual and somatosensory cortex of the macaque monkey and human brain. Journal of Comparative Neurology 297, 441–470.

McFadden, K., and Minshew, N. J. (2013). Evidence for dysregulation of axonal growth and guidance in the etiology of ASD. Frontiers in Human Neuroscience 7, article 671, 1-10. doi: 10.3389/fnhum.2013.00671

Meynert T. 1867. Der Bau der Grosshirnrinde und seine ortlichen Verschiedenheiten, nebst einem pathologischanatomischen Corollarium. *Vierteljschr Psychiat* 1, 77-93, 126-170, 198-217.

Mortazavi, F., Wang, X., Rosene, D. L., & Rockland, K. S. (2016). White Matter Neurons in Young Adult and Aged Rhesus Monkey. Frontiers in Neuroanatomy, 10, 15. http://doi.org/10.3389/fnana.2016.00015

Molnár, Z., Métin, C., Stoykova, A., Tarabykin, V., Price, D. J., Francis, F., . . . Kennedy, H. (2006). Comparative aspects of cerebral cortical development. European Journal of Neuroscience, 23(4), 921-934.

Ramon y Cajal, S (1896) Beitrag zum Studium der Medulla oblongata, des Kleinhirns und des Ursprungs der Gehirnnerven. Deutsche vom Verfasser erweiterte Ausgabe besorgt von Johannes Bresler, mit einem Vorwort von E. Mendel. ch. III: Kleinhirnrinde. pp. 21–25.Leipzig: Verlag von Johann Ambrosius Barth

Rakic, P. (1976). Prenatal genesis of connections subserving ocular dominance in the rhesus monkey. *Nature, 261*(5560), 467-471.

Ramon y Cajal, S. 1899–1904. Textura del Sistema Nervioso del Hombre y de los Vertebrados. Madrid: Imprenta y Libreria de Nicolas Moya.

Reveley, C., Seth, A. K., Pierpaoli, C., Silva, A. C., Yu, D., Saunders, R. C., … Ye, F. Q. (2015). Superficial white matter fiber systems impede detection of long-range cortical connections in diffusion MR tractography. *Proceedings of the National Academy of Sciences of the United States of America, 112*(21), E2820–E2828. http://doi.org/10.1073/pnas.1418198112

Rockland, K. S., & Nayyar, N. (2012). Association of Type I Neurons Positive for NADPH-Diaphorase with Blood Vessels in the Adult Monkey Corpus Callosum. *Frontiers in Neural Circuits*, *6*, 4. http://doi.org/10.3389/fncir.2012.00004

Schmitz, C., Eastwood, B. S., Tappan, S. J., Glaser, J. R., Peterson, D. A., & Hof, P. R. (2014). Current automated 3D cell detection methods are not a suitable replacement for manual stereologic cell counting. *Frontiers in Neuroanatomy, 8*, 27. http://doi.org/10.3389/fnana.2014.00027

Smiley, J. F., Levey, A. I., and Mesulam, M. M. (1998). Infracortical interstitial cells concurrently expressing M2-muscarinic receptors, acetylcholinesterase and nicotinamide adenine dinucleotide phosphate-diaphorase in the human and monkey cerebral cortex. *Neuroscience* 84, 755–769. doi:10.1016/S0306-4522(97)00524-1

Tomioka, R., and Rockland, K. S. (2007). Long-distance corticocortical GABAergic neurons in the adult monkey white and gray matter. *Journal of Comparative Neurolology* 505, 526–538. doi: 10.1002/cne.21504

Vogt, J., Paul, F., Aktas, O., Müller-Wielsch, K., Dörr, J., Dörr, S., . . . Zipp, F. (2009). Lower motor neuron loss in multiple sclerosis and experimental autoimmune encephalomyelitis. Annals of Neurology Ann Neurol., 66(3), 310-322.

von Engelhardt J., Khrulev S., Eliava M., Wahlster S., Monyer H. (2011). 5-HT3A receptor-bearing white matter interstitial GABAergic interneurons are functionally integrated into cortical and subcortical networks. Journal of Neuroscience. 31, 16844–1685410.1523/JNEUROSCI.0310-11.2011

Yan, X. X., Jen, L. S., and Garey, L. J. (1996). NADPH-diaphorase-positive neurons in primate cerebral cortex colocalize with GABA and calcium-binding proteins. *Cerebral. Cortex* 6, 524–529.

CURRICULUM VITAE

Daniel Lee (1991)

dandily@bu.edu | (914) 714-9233
266 E Berkeley St. APT 344, Boston, MA 02118

EDUCATION

Boston University Boston, MA
M.S., Medical Sciences Expected September 2016
Dissertation: Sulcal and Gyral Distribution of White Matter Neurons in Macaque Monkey

New York University New York, NY
B.S., Neuroscience May 2013

SCHOLARSHIPS

NYU College of Arts and Sciences (CAS) Scholarship 2009-2013
Boston University Provost Scholarship 2014

RESEARCH EXPERIENCE

Boston University Boston, MA
Master's student 2015
Advisor: Kathleen Rockland, Ph.D
Designed and carried out an investigation on the distribution of white matter neuron density for my thesis requirement. Learned laboratory techniques including cutting, staining, and mounting slides. Assisted in the technical aspects of lab like software troubleshooting.

New York University New York, NY
Research Assistant 2013
Advisor: John Rinzel, Ph.D
Scheduled and carried out investigation on spatial recognition using inter-aural time and level differences. Helped gather and analyze data as well as assisting in modifying the code for further studies.

RELATED PROFESSIONAL ACTIVITIES

Dr. Anthony Jung's Office Queens, NY

Shadowing 2015

Flushing Medical Hospital Queens, NY
Volunteer 2010